IISNC379-301X

UNIVERSITE LIBRE DE BRUXELLES - VRIJE UNIVERSITEIT BRUSSEL
INTER-UNIVERSITY INSTITUTE FOR HIGH ENERGIES

STUDY OF COHERENT PRODUCTION OF ρ^- MESONS BY CHARGED CURRENT ANTINEUTRINO INTERACTIONS IN BEBC

BEBC WA59 Collaboration

Presented by P. MARAGE

Dipartimento di Fisica dell'Università e Sezione INFN, Bari, Italy
University of Birmingham, UK
Inter-University Institute for High Energies, ULB-VUB, Brussels, Belgium
CERN, Geneva, Switzerland
Nuclear Research Centre Demokritos, Athens, Greece
LPNHE, Ecole Polytechnique, Palaiseau, France
Imperial College of Science and Technology, London, UK
Institute of Nuclear Physics, Cracow, Poland
Max-Planck-Institüt fur Physik und Astrophysik, München, Germany
Department of Nuclear Physics, Oxford, UK
Rutherford Appleton Laboratory, Chilton, Didcot, UK
DPhPE, Centre d'Etudes Nucléaires, Saclay, France
Institute of Physics, University of Stockholm, Sweden
Department of Physics and Astronomy, University College London, UK

Paper submitted to Neutrino 1986, the 12th International Conference on Neutrino Physics and Astrophysics, Sendaï - Japan

Universities of Brussels (ULB-VUB)
Pleinlaan, 2
1050 Brussels

May 1986
IIHE-86.02

Abstract.

Coherent production of ρ^- mesons by charged current antineutrino interactions on neon nuclei is studied in the BEBC bubble chamber exposed to the CERN SPS wide band beam. The corresponding cross section is measured to be $(73 \pm 23)\ 10^{-40}$ cm^2/neon nucleus, averaged over the beam energy spectrum. The distributions of kinematical variables and the absolute value of the cross-section are in agreement with theoretical predictions based on CVC and the vector meson dominance model.

1. Introduction.

The observation of coherent charged current interactions of antineutrinos on neon nuclei has been reported in a previous publication (1). In a second publication (2), we studied the dominant contribution to that signal, the production of a single pion, and compared the data in the channel

$$\bar{\nu}_\mu + Ne \rightarrow \mu^+ + \pi^- + Ne \qquad (1a)$$

to theoretical predictions based on PCAC and the meson dominance model. In the present paper, we study another exclusive channel, the coherent production of ρ^- mesons :

$$\bar{\nu}_\mu + Ne \rightarrow \mu^+ + \rho^- + Ne \qquad (1b)$$

The data come from an exposure of the bubble chamber BEBC to the antineutrino wide band beam at the CERN SPS. The chamber was filled with a 75 mole % Ne/H_2 mixture in which the radiation length is 42 cm. A total of 16000 charged current antineutrino interactions with positive muons of momentum greater than 5 GeV were selected with the external muon identifier (EMI).

The discussion of the present signal is based on the observation of 37 events of the type ($\mu^+ \pi^- \pi^\circ$) with a fully reconstructed π° meson and showing no evidence for nuclear breakup, at $|t| < 0.1$ GeV^2, where t is the square of the 4-momentum transfer to the nucleus. The background is estimated to be (9 ± 4) events. We interpret this signal as due to coherent diffractive production of ρ^- mesons on neon nuclei.

Two other experiments have searched for vector meson production in coherent (anti)neutrino interactions on heavy nuclei : three candidates were reported from an exposure of Gargamelle filled with freon to the CERN PS antineutrino beam (3), and 17 events (of which 7 were estimated to be background) were observed in an experiment at the CERN SPS neutrino beam, with Gargamelle filled with a propane-freon mixture (4). A signal for the diffractive production of ρ^+ mesons by neutrino interactions on hydrogen has been reported by two bubble chamber experiments. In (5), the events were selected among 1-C fit events of the type ($p \mu^+ \pi^- \pi^\circ$), where the gammas from the π° decay are not seen; 16 events were observed, of which 3 were attributed

to background. In (6), events with 1 or 2 seen gammas were used to extract the signal. Similar processes have also been studied in electro- and muo-production (7).

2. The signal for ρ^- coherent production.

For this analysis, the 2-prong charged current events with up to 4 gammas observed were rescanned for the possible presence of additional gammas, in order to reconstruct efficiently π° mesons coming from ρ^- decays;

$$\rho^- \rightarrow \pi^- + \pi^\circ \qquad (2)$$

Fig. 1a shows the (γ, γ) mass distribution for the 2-prong charged current events with 2 gammas (251 events); this distribution peaks at the π° mass. Fig. 2 shows the fit probability distribution obtained for these events when the gamma pair is constrained to come from the decay of a single π° meson and the fit probability P exceeds 1 %; it indicates that the measurement errors are well evaluated, and that the π° reconstruction is reliable.

Ref. (1) presents the method used for extracting the coherent signal. It is based on the fact that, in coherent interactions, the nucleus recoils as a whole, without breakup, giving events without stub, a stub being defined as a nuclear fragment or a proton of momentum less than 300 MeV. Fig. 3 shows the experimental distribution of the square of the 4-momentum transfer to the nucleus, t, for events with a μ^+, a negatively charged hadron and a fitted π°. The peak of 37 events without stub observed at $|t| < 0.1$ GeV^2 indicates coherent interactions. The background under this peak coming from incoherent interactions is obtained from the $|t|$ -distribution of events with stubs, normalised to that of events without stub in the region $|t| > 0.1$ GeV^2(±).

(±) $|t|$ is computed as $|t| = [\sum_i (E_i - p_i'')]^2 + [\sum_i \vec{p}_i^{\,T}]^2$, where E_i, p_i'' and $\vec{p}_i^{\,T}$ are the energy, the longitudinal momentum and the transverse momentum of the particle i with respect to the neutrino direction, the sum extending on all the final-state particles (see ref. 1).

The background thus estimated is small, amounting to (9 ± 4) events, and the coherent signal is (28 ± 7) events.

The (γ, γ) mass plot for all the events at $|t| < 0.1$ GeV^2 is presented on fig. 1b, the events containing stubs being shown hatched; the (π^-, π°) mass distribution for the events with $|t| < 0.1$ GeV^2 containing no stub shows a clear ρ^- signal (fig. 4).

We interpret the peak at $|t| < 0.1$ GeV^2 as due to coherent diffractive scattering on the neon nucleus of a ρ meson, coupled to the W boson, as indicated in fig. 5; the process is diffractive, i.e. takes place via Pomeron exchange, because the exchange of objects carrying isospin, like π or A_1 mesons, is forbidden on the isoscalar neon nucleus, and the exchange of ω-like objects is suppressed in the forward region corresponding to low $|t|$-values.

In order to evaluate the total cross section for ρ^- coherent production, several corrections have to be applied to the observed signal :

1. The production of coherent events with $|t|$-values above 0.1 GeV^2 is evaluated to be (24 ± 6) % with the Monte Carlo simulation presented below. The error accounts for uncertainties on the simulation of measurement errors. It could be noted that the coherent signal increases from (28 ± 7) events at $|t| < 0.1$ GeV^2 to (35 ± 11) events at $|t| < 0.2$ GeV^2, while the Monte Carlo predicts 4 events for $|t|$ between 0.1 and 0.2 GeV^2.

2. Another major correction has to account for the coherent events in which one or two gammas from the π° decay escape detection in the bubble chamber. The gamma detection efficiency is evaluated from the gamma multiplicity distribution to be (85 ± 5) % for 2-prong events. Taking into account the $|t|$-distributions, the number of coherent events with 1 detected gamma is expected to be (8 ± 4) for $|t| < 0.1$ GeV^2 and (10 ± 5) for $|t| < 0.2$ GeV^2; this is to be compared to observed coherent signals of (7 ± 7) and (16 ± 10) events respectively, including (3 ± 3) events attributed to single pion coherent production with emission of muon inner bremstrahlung (2).

3. A third important correction evaluated by the Monte Carlo simulation is the effect of the p_{μ^+} cut. The loss of events with muon momentum < 5 GeV is estimated to be (18 ± 3) % of the total number of coherent ρ^- events.

4. As in the case of single pion coherent production (2), the events with undefined charge due to an interaction of the π^- close to the vertex are discarded, and the remaining events are weighted according to the pion energy; the average weight is 1.085.

5. Two minor corrections have still to be taken into account : (i) after two different double scans for 2-prong events, the combined scanning efficiency for 2-prong events with gammas is (97 ± 3) %; (ii) (1 ± 1) apparent $\mu^+ \pi^- \pi^\circ$ coherent event is attributed to A_1^- production with one of the π° mesons from the A_1 decay escaping detection in the bubble chamber.

After applying these corrections, the cross section for ρ^- coherent production in antineutrino charged current interactions is found to be $(73 \pm 23)\ 10^{-40}$ cm^2/neon nucleus, averaged over the SPS wide band beam energy spectrum. This number is determined from the total number of charged current $\bar{\nu}_\mu$ interactions in the present experiment (taking into account the 4 % due to interactions on the H_2 in the liquid), and from the known $\bar{\nu}_\mu$ charged current cross section : $\sigma/E = (0.35 \pm 0.02)\ 10^{-38}$ cm^2/GeV (8). All the errors have been added in quadrature, including a 4 % error due to the uncertainties on the flux shape.

3. Theoretical predictions.

The form for the ρ diffractive coherent production cross section, based on the vector meson dominance model (VMD) as represented in fig. 5 is (9-12) :

$$\frac{d^3\sigma}{dQ^2\, d\nu dt} = \frac{G^2}{4\pi}\ \frac{1}{g_\rho^2}\ \left(\frac{m_\rho^2}{Q^2 + m_\rho^2}\right)^2\ Q^2\ \frac{\nu}{E^2}\ \frac{1}{1-\varepsilon}$$

$$\times\ (1 + \varepsilon R)\ \frac{d\sigma^T\ (\rho^- Ne \rightarrow \rho^- Ne)}{dt} \qquad (3)$$

where $G = 1.166\ 10^{-5}$ GeV^{-2} is the weak coupling constant; m_ρ^2/g_ρ is the coupling constant of the ρ^- meson to the intermediate vector boson, with $g_\rho = f_\rho/\sqrt{2}$ and $f_\rho^2/4\pi = 2.6$; $m_\rho = 0.775$ GeV is the ρ meson mass; Q^2 is the square of the 4-momentum transfer from the leptons to the hadrons, $\nu = E_{\nu^-} - E_{\mu^+}$,

$\varepsilon = \frac{4\,E\,(E-\nu) - Q^2}{4\,E\,(E-\nu) + Q^2 + 2\,\nu^2}$ is the polarisation parameter of the virtual intermediate boson, and $R = \frac{d\sigma^L}{dt} / \frac{d\sigma^T}{dt}$ where σ^L and σ^T are respectively the longitudinal and transverse ρ^- cross sections. Our data are mostly at $Q^2 < 1$ GeV^2 and $W > 2.5$ GeV (see fig. 8) where measured values for R are small (7). For the present comparison with the data, we take $R = 0$ and $R = \xi^2\, Q^2/m_\rho^2$, where $\xi^2 = 0.4$ (7b).

The ρ^--Ne elastic cross section is evaluated following the form proposed by Rein and Sehgal (13) for the case of single pion production :

$$\frac{d\sigma^{L,T}\,(\rho^-\,Ne \to \rho^-Ne)}{dt} = \frac{A^2}{16\pi}\;\sigma_{tot}^{2\;L,T}\;(\rho^- - N)\;e^{-b|t|}\;F_{abs} \qquad (4)$$

wher A = 20 is the neon atomic number, $\sigma_{tot}\,(\rho^-N)$ is the total ρ^--nucleon cross section at $E_\rho = \nu$, $b = 1/3\;R^2$ (R is the effective nuclear radius). The factor F_{abs} accounts for nuclear reinteractions of the ρ meson or of its decay products inside the nucleus; it is evaluated by treating the nucleus as an homogeneous sphere of radius R :

$$F_{abs} = e^{-\langle x\rangle/\lambda}\;, \quad \lambda^{-1} = \sigma_{inel}^{\rho^-N}\,.\rho\;, \qquad (5)$$

where $\langle x\rangle$ is the average path length of the meson in the nucleus, and ρ is the nuclear density : $\rho = A\,(\frac{4\pi}{3}\;R^3)^{-1}$. The value of F_{abs}, averaged over the SPS energy spectrum, is 0.45. It has been observed in (2) that, despite its crudity, the model of eq. (4)-(5) appears to reproduce the data surprisingly well; in particular, the radius of the neon nucleus extracted using (4) is (2.8 ± 0.3) fm. to be compared to the measured value of 3.0 fm. The (ρ^-N) cross section has not been measured directly, but the $(\rho^\circ N)$ cross section is known to be close to the $(\pi^\circ N)$ cross section (7); we have thus taken

$$\sigma(\rho^-N) = \sigma(\pi^-N). \qquad (6)$$

4. Comparison with the data.

The absolute value for the ρ^- coherent production cross section in two energy bins (E < 30 GeV and E > 30 GeV) is shown on fig. 6. It is compared with Monte Carlo predictions based on eq. (3-6), taking into account

measurement errors. The agreement is good, and in particular the data show the trend to an increase of the cross section with E_ν as predicted by the model in our energy range.

Differential distributions for the coherent signal are shown on fig. 7 and 8 for the variables $|t|$, t', E_ν, ν, Q^2, W, x and y, where $t' = |t| - t_{min}$, $t_{min} \simeq (\frac{Q^2 + m_\rho^2}{2\nu})^2$ is the lower kinematic limit of $|t|$, $W = (2 M_p \nu - Q^2 + M_p^2)^{1/2}$, $x = Q^2/2 M_p \nu$ and $y = \nu/E_\nu$ (M_p is the proton mass).

On these figures, the 37 events with no stub at $|t| < 0.10$ GeV^2 are displayed, and compared with the predictions of the Monte Carlo simulation based on eq. (3-6). Among those events, (76 $\pm$ 11) % are estimated to be coherent; the background is obtained from the (weighted) 5 incoherent events with stubs, and is subtracted from the distributions (the subtracted events are shown hatched). The mean values for the experimental distributions and for the Monte Carlo predictions are presented in Table I.

A good agreement is observed between the data and the predictions of the standard VMD model for all variables presented. This is true in particular for $\langle Q^2 \rangle$. Alternative forms for the Q^2 dependence, as suggested in ref. (11), have also been tested; however, the data do not support these : two of them predict significantly too low cross sections, whereas the third predicts too high $\langle Q^2 \rangle$.

Fig. 9 compares the ν, Q^2, x and y distributions for the π^- and ρ^- coherent events. Significant differences arise in ν, Q^2 and y. In particular, the sharp peaking of the Q^2-distribution at low Q^2-values for the π^- events disappears in the case of the ρ^- events; this is because CVC requires the Q^2 distribution to vanish at $Q^2 = 0$ in the case of vector meson production, whereas the abundant π^- production at low Q^2 is due to the coupling of the π^- meson to the longitudinal A_1. On the other hand, the x-distributions of the π^- and ρ^- events are similar, and essentially restricted to x-values < 0.2. This is kinematically linked to the small $|t|$-values selected for the coherent events; more generally, it is a necessary consequence of the fact that long distance hadronic fluctuations have to develop from the virtual W boson in order to interact coherently with the nucleus.

Fig. 10 presents the $\cos\theta^{\pm}$ distribution for the ($\mu^+ \pi^- \pi^\circ$) events, where $\theta^{\pm}$ is the angle between the ρ direction and the π^- direction in the ρ rest frame. Assuming s-channel helicity conservation, this distribution tests the contribution of the helicity-zero ρ production :

$$W(\cos\theta^{\pm}) = \frac{3}{4} [1 - \rho_{00} + (3\rho_{00} - 1) \cos^2\theta^{\pm}] \qquad (7)$$

The value of ρ_{00} extracted is (0.46 ± 0.22), which, for events with $\langle Q^2 \rangle$ = 1.2 GeV^2, agrees well with electro- and muo-production data (7).

4. Conclusion.

In conclusion, using BEBC exposed to the CERN SPS $\bar{\nu}_\mu$ wide band beam, we have pursued the study of the exclusive channels contributing to the coherent charged current antineutrino interactions by the analysis of the coherent production of ρ^- mesons. The corresponding cross section is measured to be $(73 \pm 23)\ 10^{-40}$ cm^2/neon nucleus, averaged over the beam energy spectrum. The distributions of kinematical variables and the absolute value of the cross section are in agreement with theoretical predictions based on CVC and the vector meson dominance model.

Acknowledgments.

We are pleased to acknowledge the excellent work of the SPS, BEBC and EMI crews during the run; we also thank our scanning and measuring teams for their carefull work.

References.

(1) P. MARAGE et al., Phys. Lett. 140B (1984) 137.

(2) P. MARAGE et al., Coherent Single Pion Production by Antineutrino Charged Current Interactions and Test of PCAC, submitted to this Conference and to be publ. in Zeit. Phys. C.

(3) D. PICARD, Production Cohérente des Mésons-Vecteurs dans l'Expérience Wide-Band du PS, Orsay, LAL-79/38 (1979).

(4) A. BOUCHAKOUR, Thesis, Strasbourg (1980).

(5) J. BELL et al., Phys. Rev. Lett. 40 (1978) 1226.

(6) D.R.O. MORRISON, Proceedings of the 1978 International Meeting on Frontier of Physics, ed. by K.K. Phua, C.K. Chew and Y.K. Lim, Singapore National Academy of Science (1978), 205.

(7) a. T.H. BAUER et al., Rev. Mod. Phys. 50 (1978), 261 and references therein;
b. J.J. AUBERT et al., Phys. Lett. 161B (1985), 203 and references therein.

(8) M. ADERHOLZ et al., to be published in Phys. Lett.

(9) C.A. PIKETTY and L. STODOLSKY, Nucl. Phys. B15 (1970), 571.

(10) M.K. GAILLARD, S.A. JACKSON and D.V. NANOPOULOS, Nucl. Phys. B102 (1976), 326.

(11) M.S. CHEN, F.S. HENYEY and G.L. KANE, Nucl. Phys. B118 (1977), 345.

(12) A. BARTL, H. FRAAS and W. MAJEROTTO, Phys. Rev. 16D (1977), 2124.

(13) D. REIN and L.M. SEHGAL, Nucl. Phys. B223 (1983) 29.

Table 1.

	Data	Model
$E_{\bar{\nu}}$ (GeV)	30.9 ± 3.8	36.1
P_{μ} (GeV)	20.6 ± 3.1	23.1
ν (GeV)	10.2 ± 2.3	13.0
p_{π^-} (GeV/c)	5.2 ± 1.5	7.3
p_{π° (GeV/c)	5.1 ± 1.2	5.8
Q^2 (GeV^2)	1.19 ± 0.31	1.16
W (GeV/c^2)	4.04 ± 0.40	4.59
x	0.074 ± 0.017	0.053
y	0.305 ± 0.041	0.381
$m(\pi^-,\pi^\circ)$ (GeV/c^2)	0.723 ± 0.040	0.750

Table 1 : Mean values of kinematical variables for the coherent $\mu^+ \pi^- \pi^\circ$ events with $P_{\mu^+} > 5$ GeV and $|t| < 0.1$ GeV^2, after background subtraction, compared to the predictions of the model (eq. 3 to 6), including the effects of experimental resolution; errors of the order of a few % arise on the model predictions for several variables because of the uncertainty on the flux shape; the parameter R in (3) is taken here to be 0.

Figure captions.

Fig. 1 : Distribution of the (γ, γ) mass for events with a μ^+, a π^- and 2 γ's a) all events (251 events); b) events at $|t| < 0.1$ GeV^2 (42 events; the 5 events with stubs are shown hatched).

Fig. 2 : Distribution of π° fit probability for the events with a μ^+, a π^- and 2 γ's, where the γ pair is constrained to come from the decay of a single π° meson with a probability $P > 1$ %.

Fig. 3 : Distribution of the square of the 4-momentum transfer $|t|$ for 121 ($\mu^+ \pi^- \pi^\circ$) events without stub and for 53 events with stubs, normalised to the former for $|t| > 0.1$ GeV^2.

Fig. 4 : Distribution for the (π^-, π°) mass for 37 ($\mu^+ \pi^- \pi^\circ$) events without stub at $|t| < 0.1$ GeV^2; the incoherent background, estimated from the corresponding events with stubs, is shown hatched. The curve, - normalised to the coherent signal -, is the prediction of the model (eq. 3 to 6), including the effects of experimental resolution.

Fig. 5 : Coherent diffractive production of a ρ^- meson by $\bar{\nu}_\mu$ charged current interaction on neon nucleus.

Fig. 6 : Cross section for ρ^- coherent production by $\bar{\nu}_\mu$ charged current interactions on neon nuclei, as a function of the $\bar{\nu}$ energy $E_{\bar{\nu}}$; the curve is the prediction of the simulation presented in the text (eq. 3 to 6), including the effects of experimental resolution, using $R = 0$ (solid line) and $R = \xi^2 Q^2/m_\rho^2$, with $\xi^2 = 0.4$ (dashed line).

Fig. 7 : Distributions for a) the square of the 4-momentum transfer t; b) $t' = |t| - t_{min}$ for the $\mu^+ \pi^- \pi^\circ$ coherent events at $|t| < 0.1$ GeV^2, weighted for the loss of events with undefined charge; the incoherent background, estimated from the events with stubs, is shown hatched. The curve, - normalised to the coherent signal -, is the prediction of the model (eq. 3 to 6), including the effects of experimental resolution.

Fig. 8 : Distributions for a) E_ν: b) $\nu = E_\nu - E_{\mu^+}$; c) Q^2; d) $W = (2 M_p \nu - Q^2 + M_p^2)^{1/2}$; e) $x = Q^2/2M_p\nu$; f) $y = \nu/E_\nu$ for the ($\mu^+ \pi^- \pi^\circ$) coherent events with $|t| < 0.1$ GeV^2, weighted for the loss of events with undefined charge; the incoherent background, estimated from the events with stubs, is shown hatched. The curve, - normalised to the coherent signal -, is the prediction of the model (eq. 3 to 6), including the effects of experimental resolution; the parameter R in (3) = 0, except for the dashed curve in c), where $R = \xi^2 Q^2/m_\rho^2$, with $\xi^2 = 0.4$

Fig. 9 : Distributions for a) ν; b) Q^2; c) x; d) y for the $\mu^+ \pi^-$ coherent events (solid histogram) and the $\mu^+ \pi^- \pi^\circ$ coherent events (dashed histogram), normalised to each other.

Fig. 10 : Distribution of $\cos\theta^*$, the angle between the ρ meson direction and the π^- direction in the ρ rest frame, for the $\mu^+ \pi^- \pi^\circ$ coherent events with $|t| < 0.1$ GeV^2 weighted for the loss of events with undefined charge; the incoherent background, estimated from the events with stubs is shown hatched.

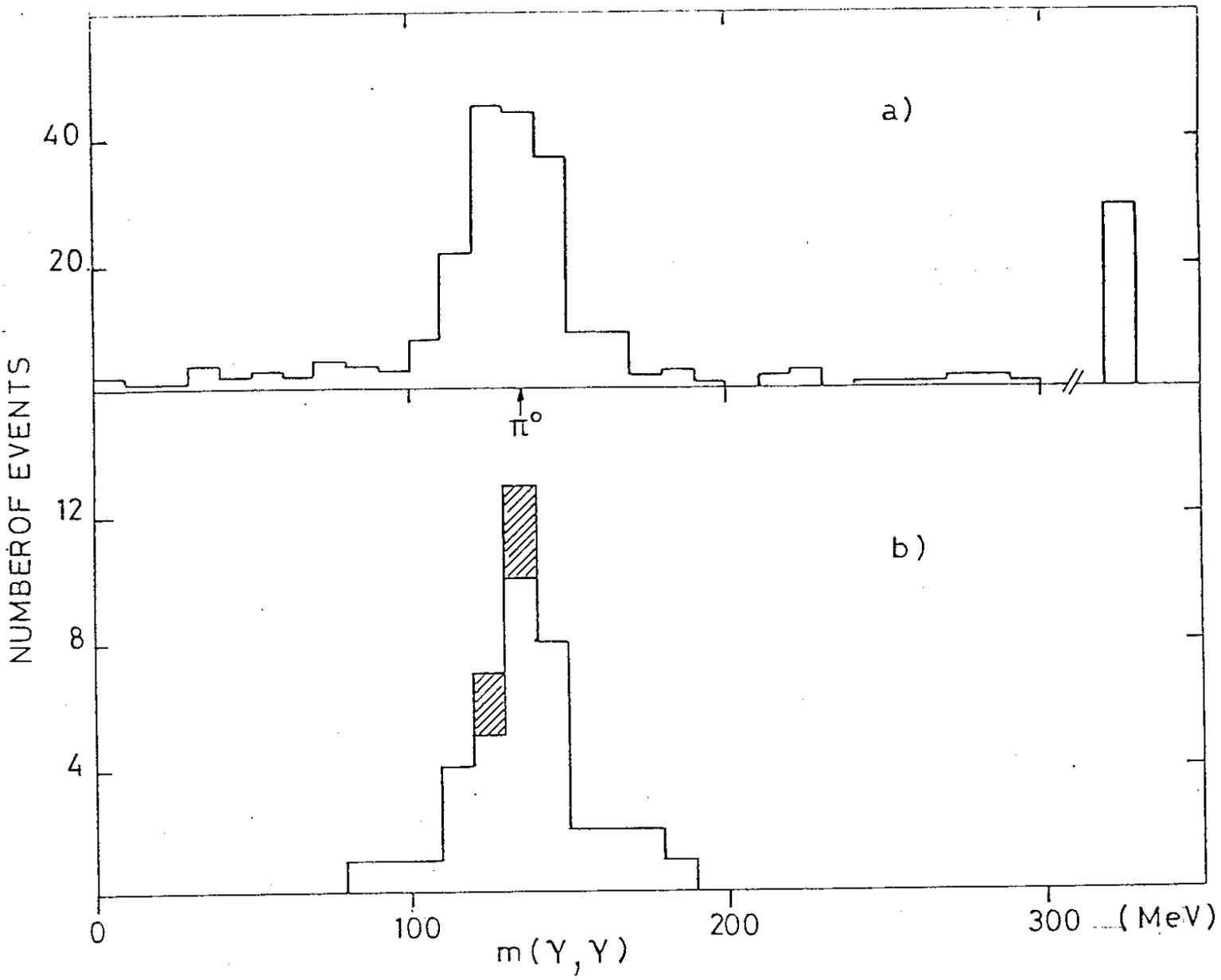
a)
40
20
NUMBER OF EVENTS
π°
12
8
4
b)
0
100
200
300
(MeV)
m(Y, Y)

Fig. 1

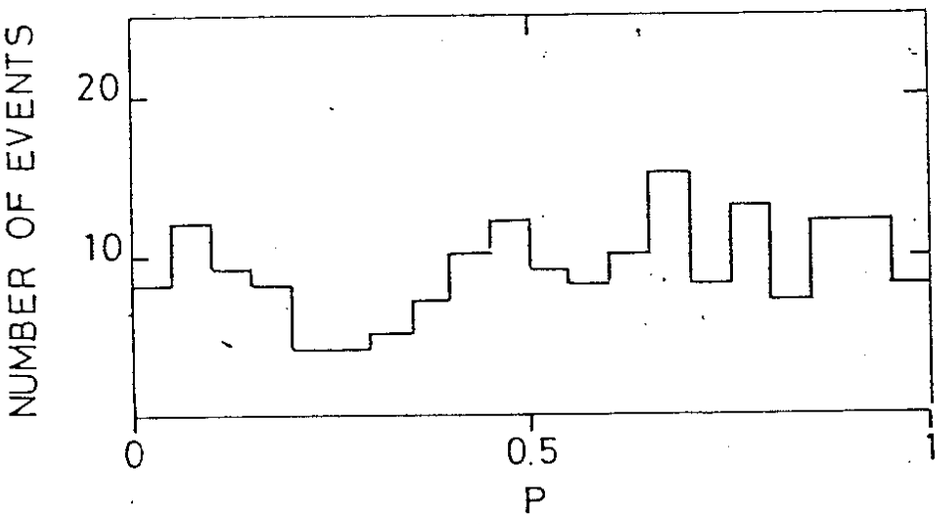
NUMBER OF EVENTS
20
10
0
0.5
1
P

Fig. 2

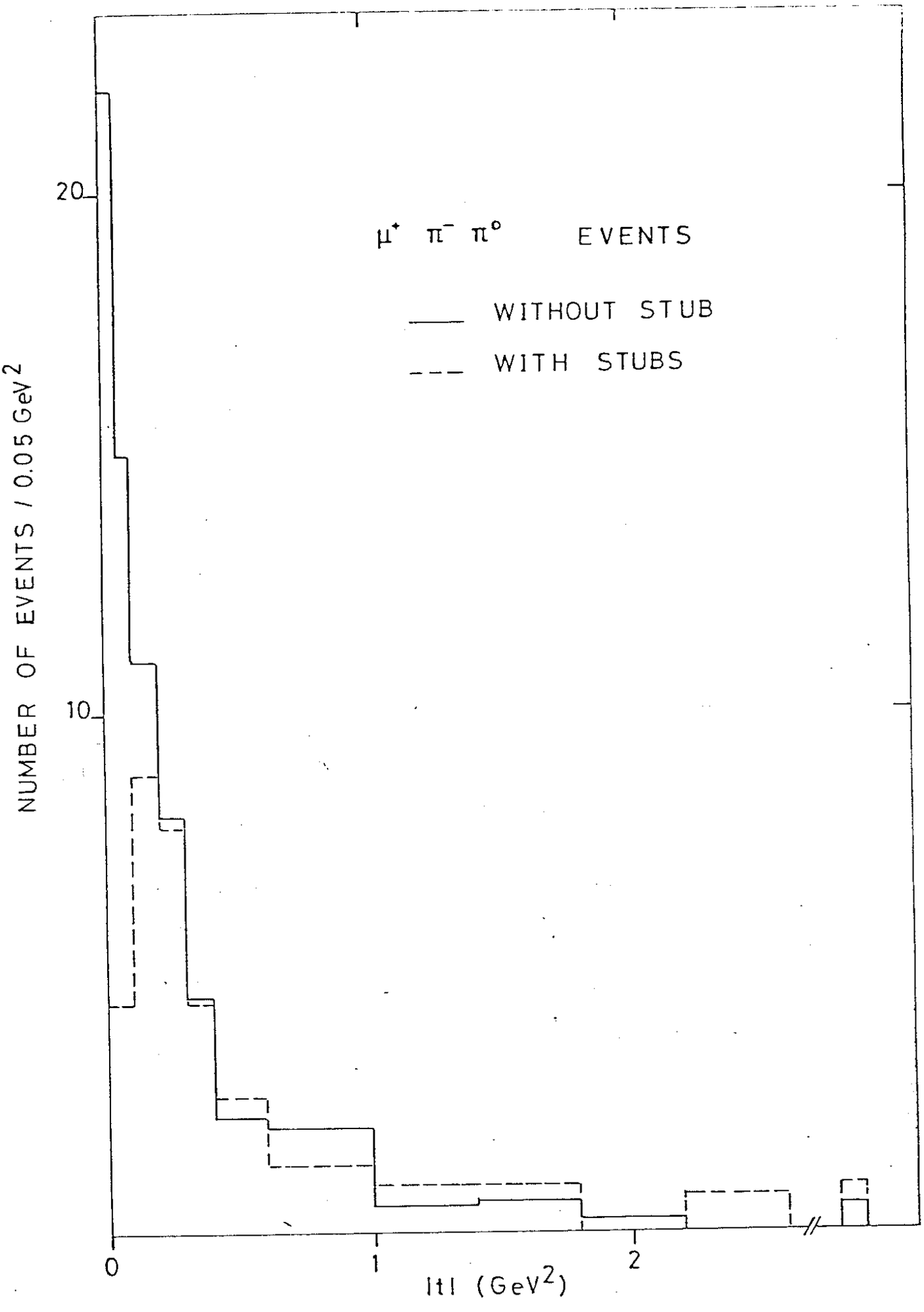
$\mu^+ \pi^- \pi^\circ$ EVENTS
WITHOUT STUB
WITH STUBS
NUMBER OF EVENTS / 0.05 GeV^2
20
10
0
1
2
|t| (GeV^2)

Fig. 3

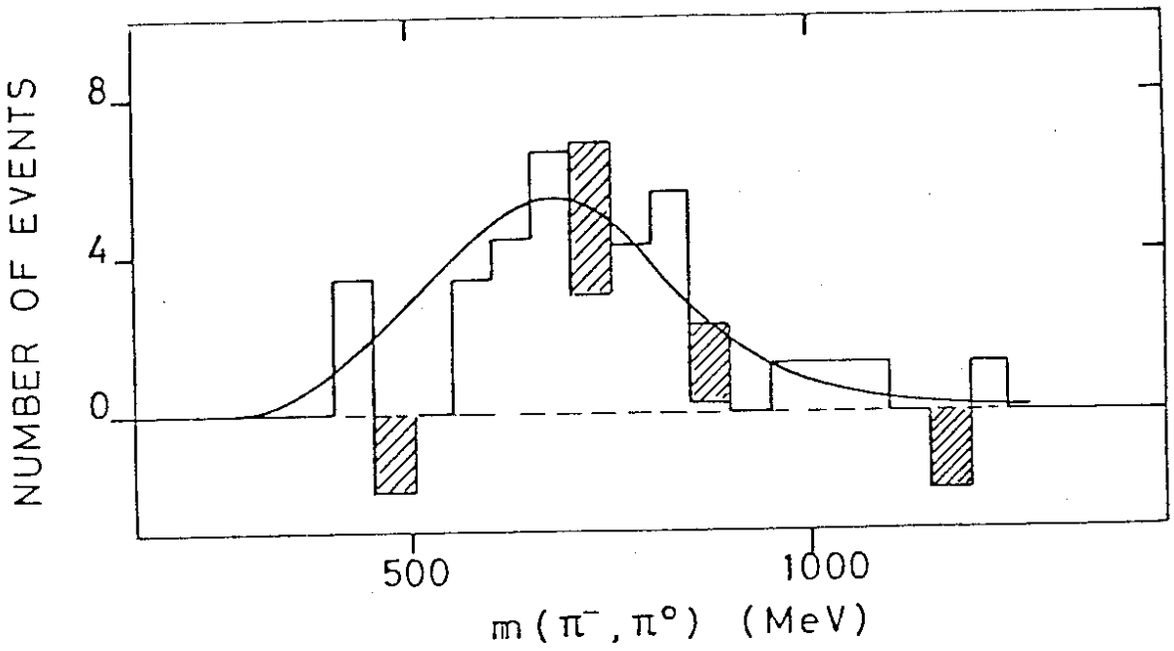

Fig. 4

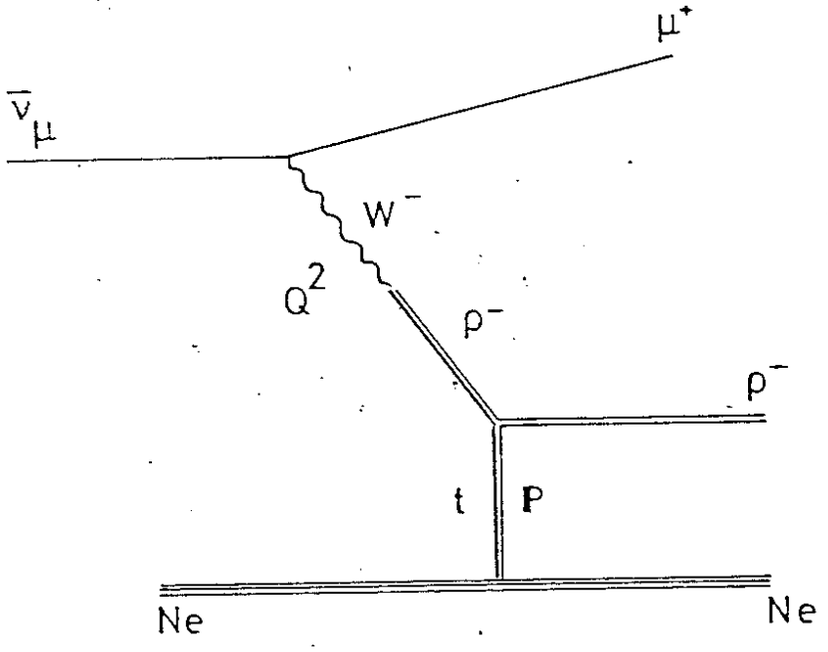

Fig. 5

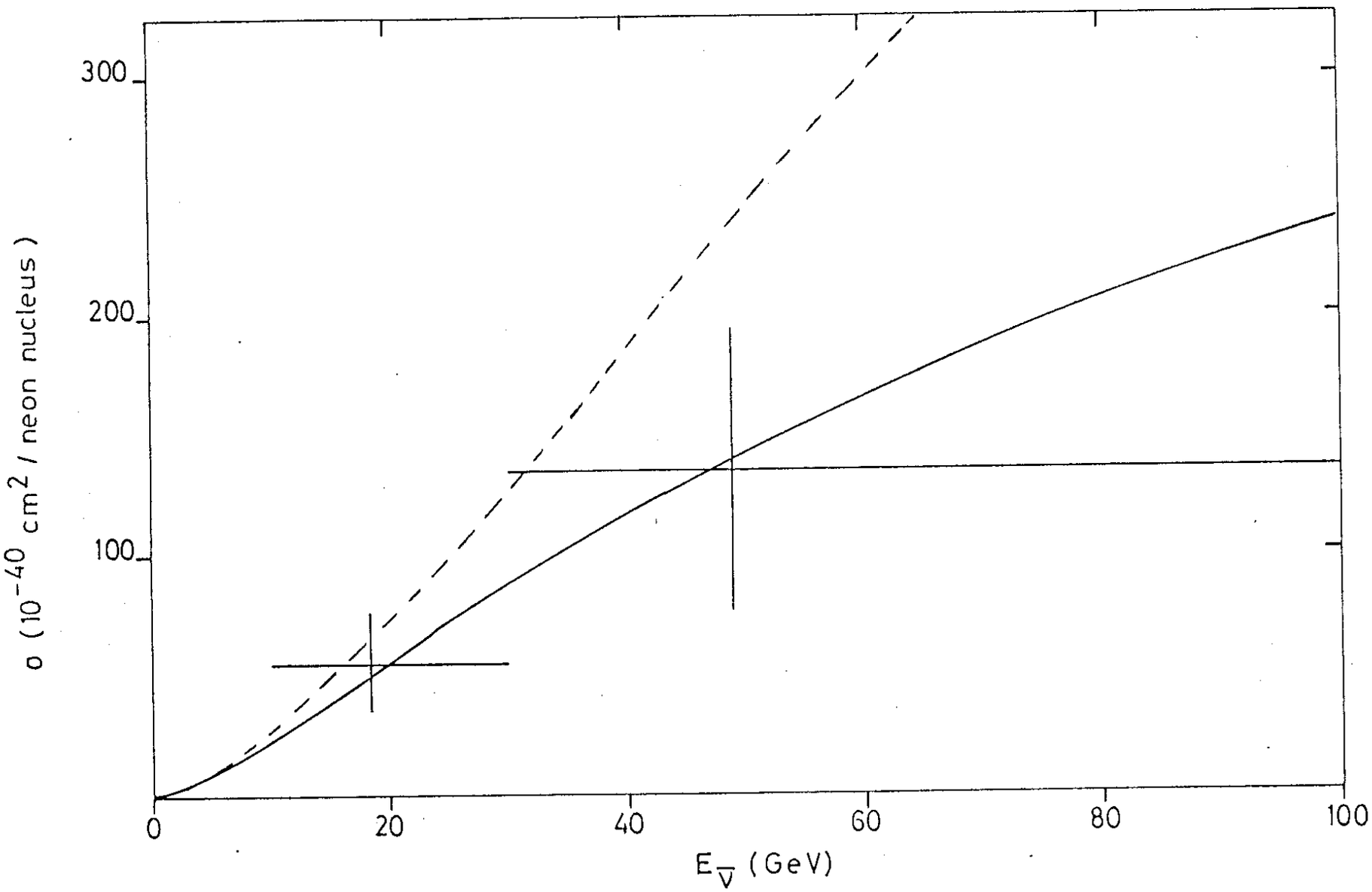

Fig. 6

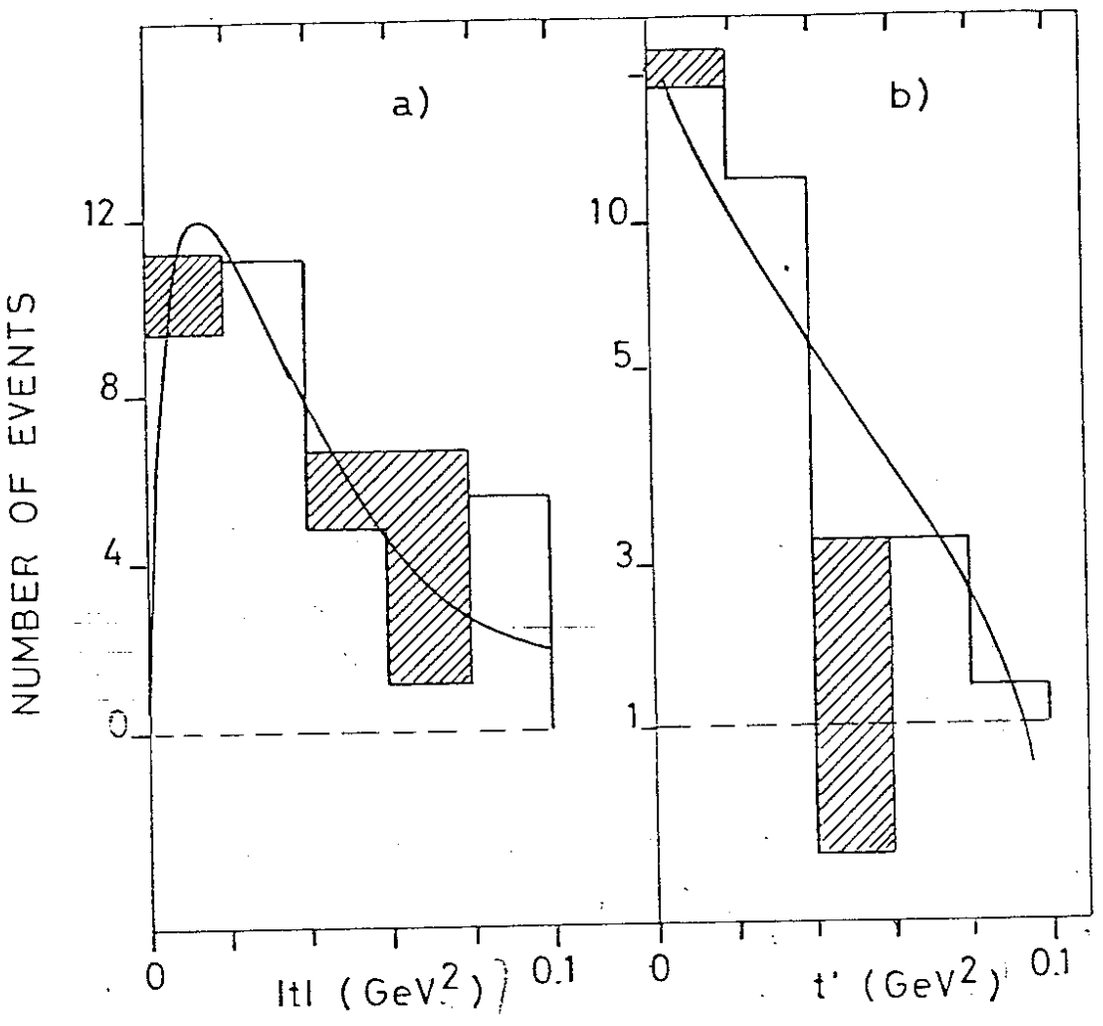

Fig. 7

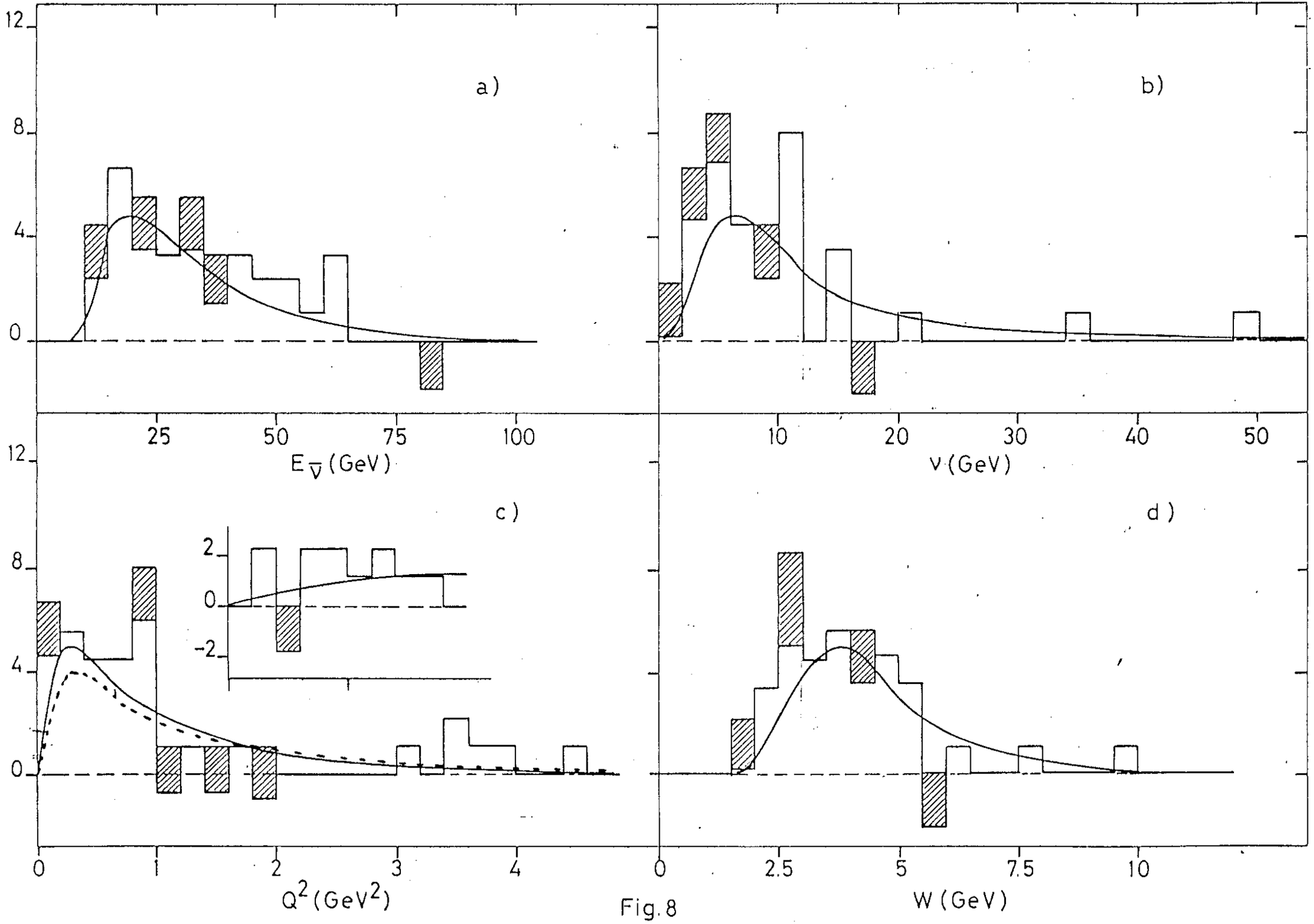

Fig. 8

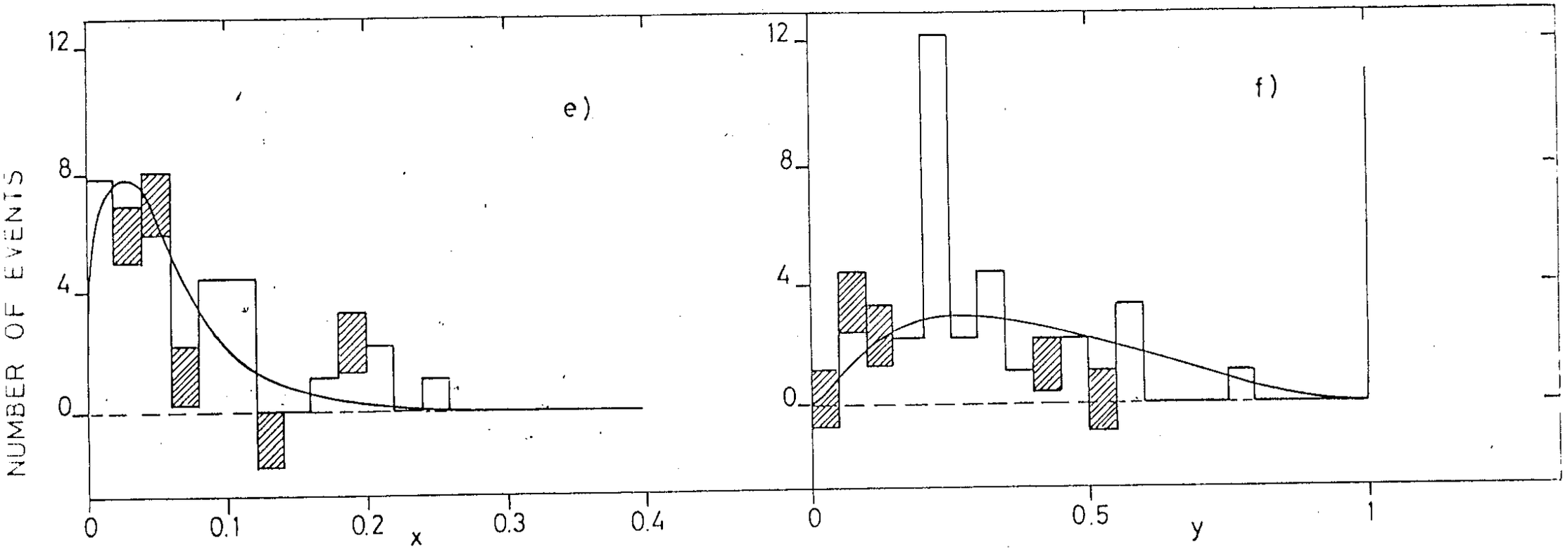

Fig. 8

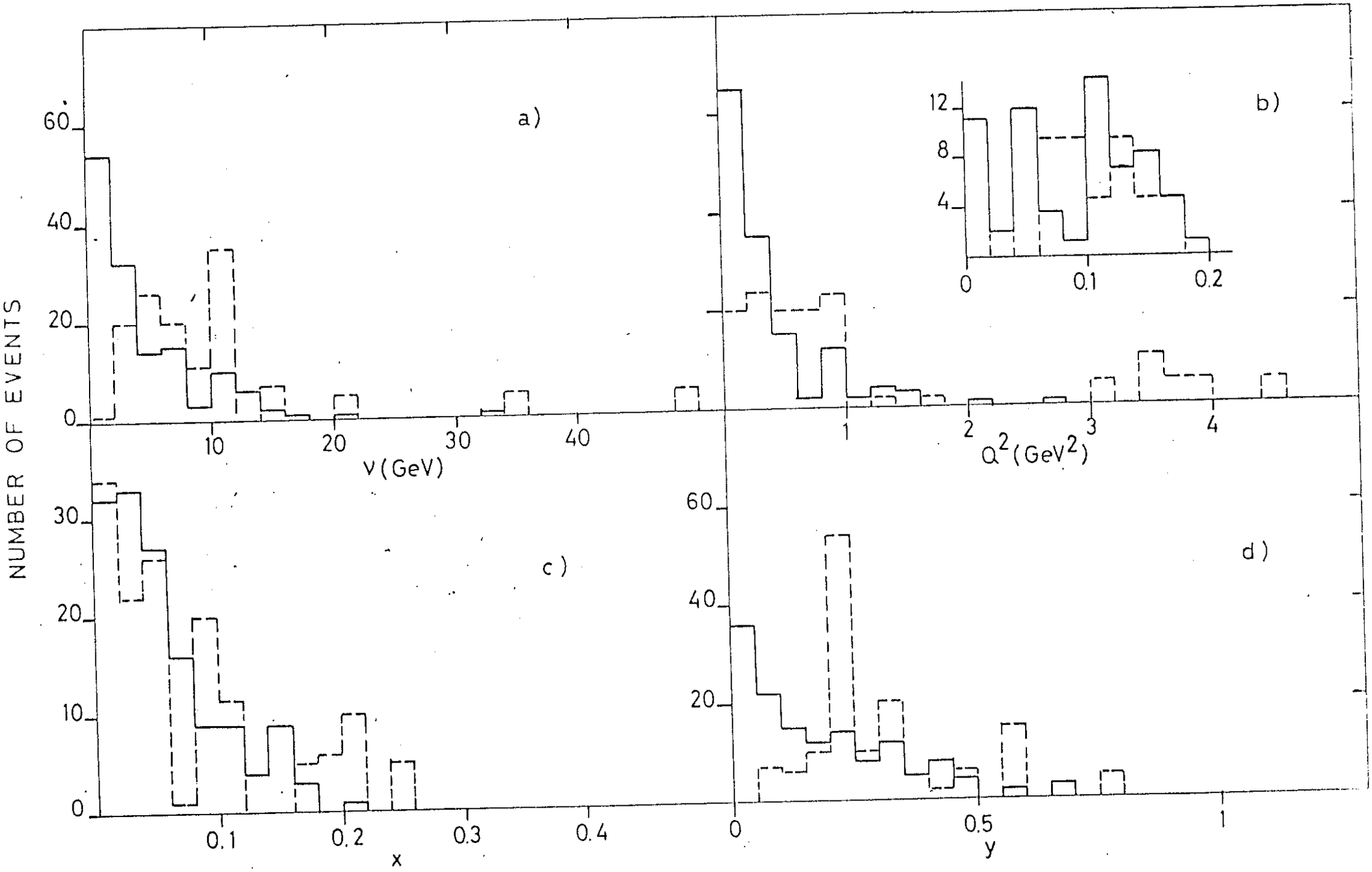
a)
b)
c)
d)
NUMBER OF EVENTS
ν (GeV)
Q^2 (GeV^2)
x
y
60
40
20
0
10
20
30
40
1
2
3
4
12
8
4
0
0.1
0.2
30
10
0.3
0.4
0.5

Fig. 9

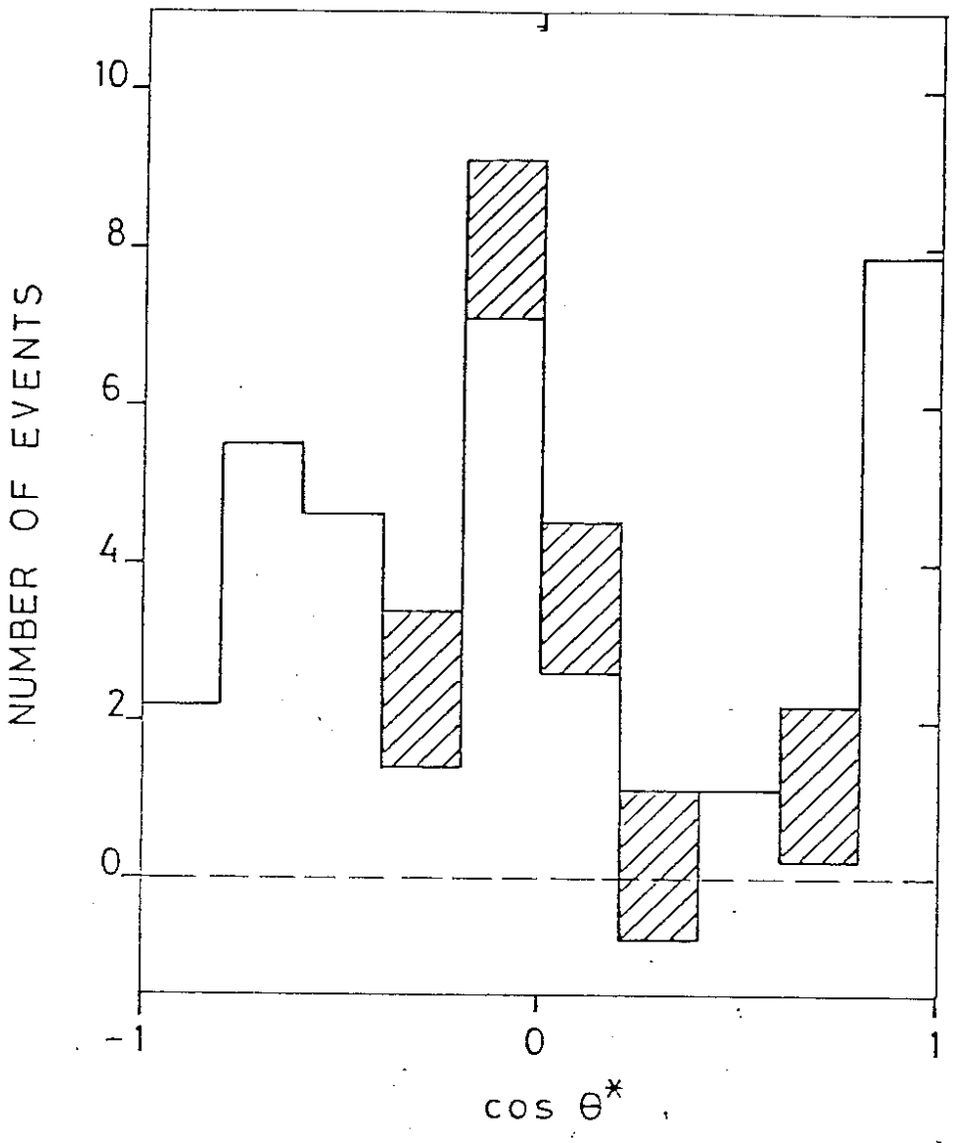

Fig. 10